RESILIENT INFRASTRUCTURE
June 1–4, 2016
RESILIENT INFRASTRUCTURE LONDON 2016

BEHAVIOR OF CIRCULAR FRP-REINFORCED CONCRETE COLUMNS UNDER ECCENTRIC LOADING

Abdeldayem HadHood,
Ph.D. Candidate, Université de Sherbrooke, Canada

Hamdy M. Mohamed
Postdoctoral Fellow, Université de Sherbrooke, Canada

Brahim Benmokrane
Professor, Université de Sherbrooke, Canada
NSERC Research Chair in FRP Reinforcement for Concrete Infrastructure
Tier-1 Canada Research Chair in Advanced Composite Materials for Civil Structures

ABSTRACT

This paper presents the results of an investigation of the eccentric compression behavior of three full-scale circular concrete columns reinforced with the glass-fiber-reinforced polymer (GFRP) bars and spirals. The column specimens measured 1500 mm height, 305 mm diameter and were tested under monotonic eccentric loading. The main variable was the eccentricity-to-dimeter ratio. Three values were considered in this study (8.20%, 16.39%, and 65.57%). The failure mechanism was changeable according to the level of the applied eccentricity. The failure mechanism of columns at small eccentric loading was defined as compression-controlled due to concrete crushing. At high eccentric loading, the failure of the column cannot simply be characterized by a compression failure, it was rather controlled by the properties of the GFRP bars. The test results were plotted to obtain the experimental P-M interaction diagram. Finally, the experimental results were analyzed and compared with predicted results.

Keywords: concrete columns; eccentric; interaction-diagram; GFRP bars

1. INTRODUCTION

Reinforced concrete has been considered the prime construction material for long years due to its reliability and long-life time. However, due to the aggressive environment especially in North America, natural chemical reactions accusing steel corrosion, threaten the safety of the whole concrete structures. Corrosion has been reported as a serious problem in concrete bridge columns/piers when subjected to de-icing salts and/or aggressive environments. Subsequently, it constitutes an important cause of structures deterioration, leading to extravagant repairs and rehabilitation as well as a significant reduction in the service lifetime. Nowadays, fiber-reinforced- polymer (FRP) materials have emerged as an alternative material for producing reinforcing bars for concrete structures (ACI 440.1R-15). FRP bars offer many advantages over conventional steel bars; a density of one-quarter to one-fifth that of steel, greater tensile strength than steel and no corrosion even in harsh chemical environments (Rizkalla et al. 2003; El-Salakawy et al. 2003; Benmokrane et al. 2006 and 2007; Mohamed and Benmokrane 2012).

Recent years have seen valuable research work and widespread applications of FRP bars as flexural and shear reinforcement for concrete structures (El-Salakawy et al. 2003; Benmokrane et al. 2006; ISIS Canada 2009; Hassan et al. 2013; Mohamed and Benmokrane 2016). Also, more recently, utilizing FRP bars and spirals in columns to resist the axial load and/or flexural moment is now under investigations (Tikka et al. 2010; Tobbi et al. 2012, Afifi at al. 2013; Zadeh and Nanni 2013; Xue et al. 2014). ACI 440.1R-15 highlights that further research is needed for columns. AASHTO (2009) stated that the strength of any FRP bars in compression shall be ignored in design calculations. Current guidelines and codes of practice do not recommend the use of FRP bars as internal reinforcement in either compression members or eccentrically-compression loaded members. However, standards

and guides (ACI 440.1R-15; CSA S806-12; CSA S6-06-10) allow using FRP bars in the compression zone of flexural members, provided that they are neglected in determining the member's axial or flexural strength. The present study attempts to enrich the technical knowledge about the behavior of circular FRP-reinforced concrete columns.

2. EXPERIMENTAL PROGRAM

2.1 Specimens Details

In this study, three full-scale circular GFRP-RC columns were prepared and tested under monotonically increasing eccentric loading. All specimens have 305 mm (12") diameter and 1500 mm (60") height, they were reinforced longitudinally by 8 GFRP No. 5 (15.9 mm) and transversely with GFRP spiral No.3 (9.5 mm) each 80mm. The test parameters included three eccentricity-to-diameter ratios (0, 8.2, 16.4, and 65.6%) to achieve all possible failure modes. The longitudinal and transverse reinforcement were designed to satisfy the minimum and maximum limits of the standard codes (1% and 8%). GFRP cages were assembled for the different column configurations, as shown in Fig. 2. Each coil of GFRP spiral reinforcement consisted of one complete helical spiral without any lapped splices. The pitch in the spiral was reduced to 50 mm outside the free region at both ends of the columns (250 mm in length) to avoid premature failure. The concrete cover was kept constant at 25 mm to the face of the spirals. The circular columns were prepared for vertical casting in very stiff Sonotubes. Wooden formworks were used to hold the Sonotubes plumb. Then, the GFRP cages were inserted into the formwork inside the Sonotubes. All columns were cast vertically to simulate the typical construction practices of columns and piles. The concrete was provided by a local ready-mix concrete company. The concrete was discharged into the column forms directly from the ready-mix concrete truck in approximately three lifts; an internal electric vibrator was used to consolidate the concrete and to remove air bubbles.

Table 1: Test matrix and specimen details

Specimen	e (mm)	e/D (%)	Longitudinal Bars		Transverse Spiral		
			ρ_f %	No.	ρ_{sp} %	No.	pitch (mm)
C25	25	8.2					
C50	50	16.39	2.18	8 No.5	0.95	3	80
C200	200	65.57					

2.2 Material Properties

Sand-coated GFRP bars and newly developed GFRP spiral were used to reinforce the GFRP-RC column specimens in the longitudinal and transverse directions, respectively. The GFRP longitudinal bars and spirals were made of continuous E-glass fibers impregnated with a thermosetting vinyl-ester resin, additives, and fillers with a fiber content of approximately 80.0% (by weight according to Standard Test Methods for the constituent content of composite materials, ASTM D3171-11). The GFRP reinforcement had a sand-coated surface to enhance bond performance between the bars and the surrounding concrete (Pultrall Inc. 2012). No. 5 (15.9 mm) GFRP bars were used as longitudinal reinforcement for all the GFRP RC columns. No. 3 (9.5 mm) GFRP spirals were used as transverse reinforcement. The tensile properties of longitudinal FRP bars were determined according to ASTM D7205 as reported in Table 2. All column specimens were cast on the same day with normal-weight, ready-mixed concrete with an average compressive strength of 35 MPa. The actual compressive strength was determined based on the average test results of 10 concrete cylinders (150 x 300 mm) tested on the same day as the start of testing of the column specimens.

Table 2: Mechanical properties of the GFRP reinforcement

Bar Size	Diameter (mm)	Area (mm^2)	Elastic Tensile Modulus (GPa)	Tensile Strength (MPa)	Tensile Strain (%)
# 3	9.5	71	52.5±2.5	f_{fu} = 1171	2.30
# 5	15.9	199	54.9±2.5	f_{fu} = 1289	2.40

Figure 1: GFRP cages, (a) internal instrumentations; (b) cages inside wooden formwork

2.3 Instrumentation and Test Setup

Specimens were instrumented by fixing Electric strain gauges to measure strains in the longitudinal bars, spirals, and concrete surfaces. Besides, linear potentiometers (LPOTS) were mounted to measure the axial and lateral displacements. Before casting, as shown in Fig. 1, strain gauges were fixed on the outermost longitudinal bars and spirals at both the tension side and the compression side. Before testing by at least 24 hours, concrete gauges were fixed on the compression side. All gauges were located on the columns mid-height at the positions where the maximum strains were expected. Before testing, LPOTS were mounted vertically at the head ram to measure the axial displacement, while others were laterally mounted at the tension and compression sides to measure the lateral displacement at the mid-height and quarter-height levels.

Before the testing process, the top and bottom surfaces were leveled to ensure a uniform load distribution. The columns were placed on pre-designed steel leveling plates which adjust the leveling process, and then a thin grout layer was cast on that surface. The next day, the columns were flipped to level the other surface. The eccentric-loading set-up consisted of two pre-designed rigid steel end caps (250mm height) in a tubular shape, see Fig. 2. Each end cap was bolted to a 40 mm diameter roller bearing. The end cap composed of two units; the first consisted of a 25 mm flat plate welded to a 15 mm semicircular plate. Meanwhile, the other unit was a 15 mm semicircular plate coincident and clamped to the first unit by 3 M15 mm bolts at each side. This set-up was fabricated from high strength steel. The whole assembly was stiffened and welded with 25 mm outward radiating stiffeners. The eccentricity was adjusted for each specimen by changing the position of the roller bearing. So, the loading was applied through the Knife-edge representing by the roller bearing at the column edges. The specimens were tested using a 6,000 kN capacity Forney machine located at Construction Facilities Laboratory of Department of Civil

Engineering, University of Sherbrooke. They were placed vertically to be coincident with the machine center of loading. The Forney machine, strain gauges, and LPOTS were connected by channels to the Data Acquisition System. The loading rate was ranged between 1.0 to 1.5 kN/s during the test by manually control the hydraulic pump.

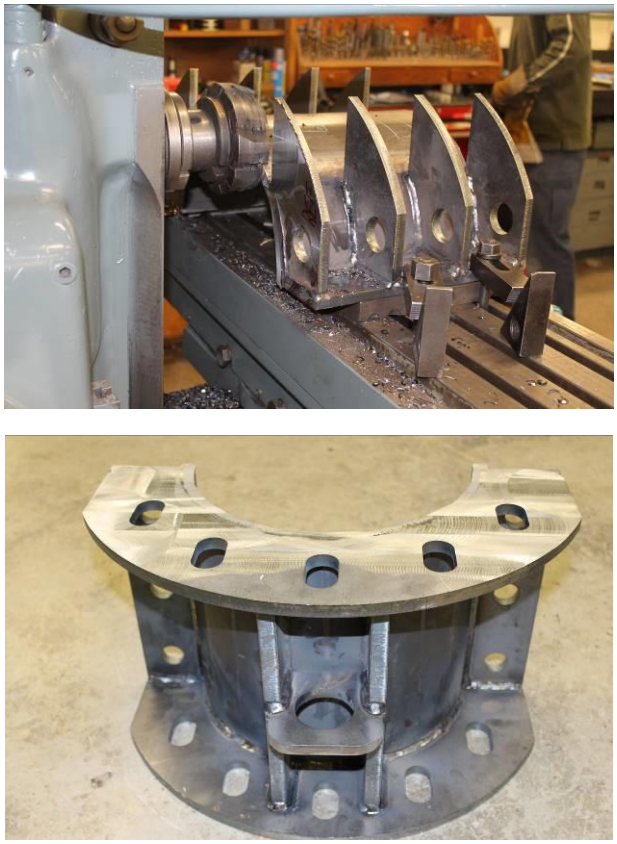

Figure 2: Rigid steel end-caps (fabrication process)

3. EXPERIMENTAL RESULTS

3.1 Cracks and Failure Mode

Based on the test results and test observations, three types of cracks were reported in this study: the first type was formed inside the concrete core at the compression side due to a state of high compressive stresses. It can be recognized from the load-concrete strain and load-displacement responses as it changes the initial stiffness, it can be called "the micro-cracks." The second type was vertically formed on the concrete shell at the compression side just before the cover spalling; it could be known as "the flexural-compression cracks." The last type was formed horizontally on the tension side of the concrete shell when concrete reaches the rupture stress (f_r), these cracks were perpendicular to the direction of the maximum principal tensile stress induced by the bending moment, this type could be known as "the flexural-tension cracks."

The load carrying capacity of the eccentric columns increased steadily but at different rates, depending on the level of eccentricity-to-diameter ratio, from the origin to a point where microcracks initiated. While the microcracks were propagating inside the concrete core, the strength gradually increased at a lower rate. Then, flexure–compression cracks initiated at a load level of 90% to 95% on the compression side at the column mid-height. On the tension side, the flexural–tension cracks initiated at different load levels (according to the level of the eccentricity-to-diameter ratio), which helped reduce the rate of the strength gain. When the peak load had been reached, the existing cracks along with the bar deformation contributed to splitting the concrete cover, causing cover spalling and,

consequently, a stress increase in the concrete core. The failure mechanism of C25 and C50 was defined as compression-controlled due to concrete crushing. Meanwhile, the failure of C200 was initiated by mild cover spalling, followed by concrete degradation. The failure of the column, however, cannot simply be characterized by a compression failure, it was rather controlled by the properties of the GFRP bars. At the peak, the strain of the GFRP bars progressively increased where the load was almost constant. While the axial and lateral displacements were progressively increasing, the concrete degradation increased. Before getting the ultimate strain of the GFRP bars, the test was halted due to safety reasons. The failure of GFRP bars under this extreme strain (the ultimate tensile strain) could cause catastrophic damage to the specimen. The maximum axial forces sustained by these specimens—C25, C50, and C200—were 2100, 1485, and 354 kN, respectively.

Figure 3: Final crack pattern of specimen C25

3.2 Axial-Displacement Response

Load versus axial displacement response for the eccentric columns is shown in Fig. 4. The axial displacement was measured by two linear potentiometers (LPOTS) mounted on the ram head. A noticeable decrease in the initial axial stiffness was observed with each increase of the eccentric loading. Generally, an initial linear branch was observed up to a load level of approximately 70% for columns C25; 65% for columns C50; and 40% for columns C200. After this stage, a semi-linear ascending branch was developed to the peak load. This branch was characterized by a loss of the initial stiffness, mainly due to the propagation of the micro-cracks on the compression side and the flexural-tension cracks (for the column tested under high eccentric loading). It was observed that the axial displacement at the peak increased as much as the eccentric loading increased. After the peak, variable strength decay was developed according the eccentric loading applied. The axial displacement was then increasing linearly while the load was constant. The response of the load-axial displacement after the peak showed a distinct deformable manner due to the high ultimate strain of the GFRP reinforcement.

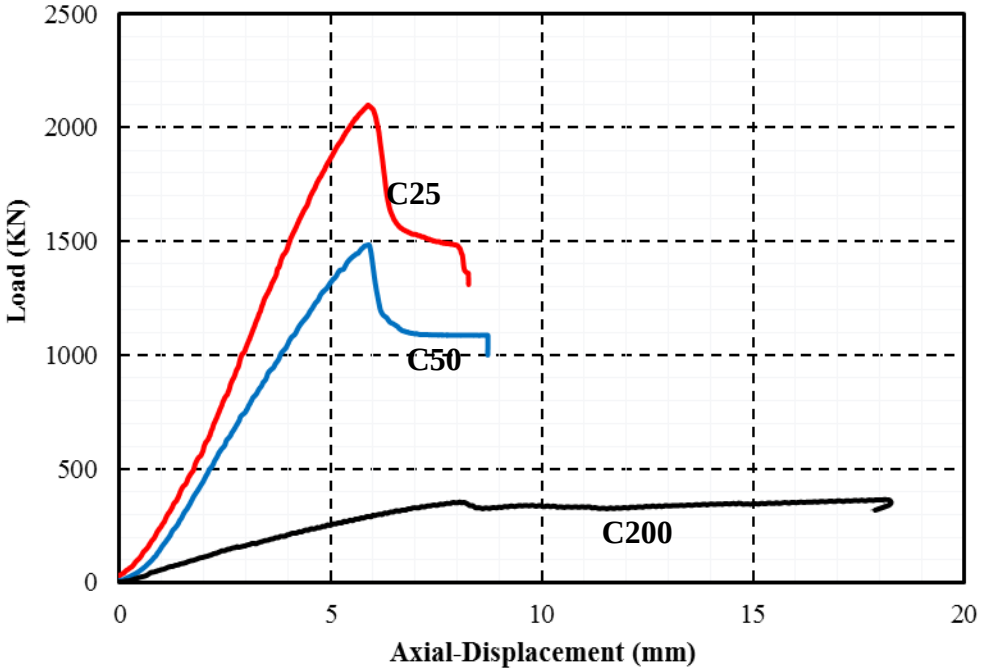

Figure 4: Load Axial-Displacement response

3.3 Effect of Load-Eccentricity

The effect of the load eccentricity was evident in all the relationships. A noticeable change in the failure mechanism was reported each time the eccentricity increased. At small eccentricity, the failure was brittle, and a massive volume of the concrete cover spalled. This mode of failure changed and became more deformable as much as the eccentricity is increased. It was observed that the eccentricity had a significant effect on the ultimate load, as should expect. The initial axial and lateral stiffness of the tested columns decreased with each increase in the eccentricity. The average axial displacement, at the peak, was 6.05, 6.1, and 9.15 mm for eccentricity to diameter ratio of 8.2%, 16.39%, and 65.57%, respectively. While the average lateral deformations, at the peak, were 4.25, 5.75, and 10.75 mm for the ratios above, respectively. In the meantime, the measured bar strains on the tension side (at the peak) noticeably increased with each increase in the eccentricity. On the other hand, the post-peak behavior for each eccentric loading was different. After the peak, the strength decayed due to the cover spalling; this decay was pretty much higher when specimens subjected to lower eccentric loading and the vice versa.

3.4 Interaction Diagram

Figure 5 shows the experimental P-M relationship of the tested specimens. The developed interaction diagram was similar in shape to the interaction diagrams of the steel-RC columns. A comprehensive analysis was carried out to predict the nominal axial and flexural resistance of this section. The analysis based on the stress block provided by the Canadian building codes (CSA CAN S806-12 and CSA CAN A23.3-14), satisfying the forces equilibrium, setting the material resistance factors to the unity and neglecting the compression contribution of the GFRP bars. The results of this analysis were compared to the experimental results. It was revealed from the comparison that the test results gave an upper bound, which means that all the predicted results were on the safe side. It was observed that the estimation of the axial force and the corresponding bending moment using the codes above was conservative. The average ratio of the experimental axial load to the predicted axial load (Pexp/Ppred) was 1.25.

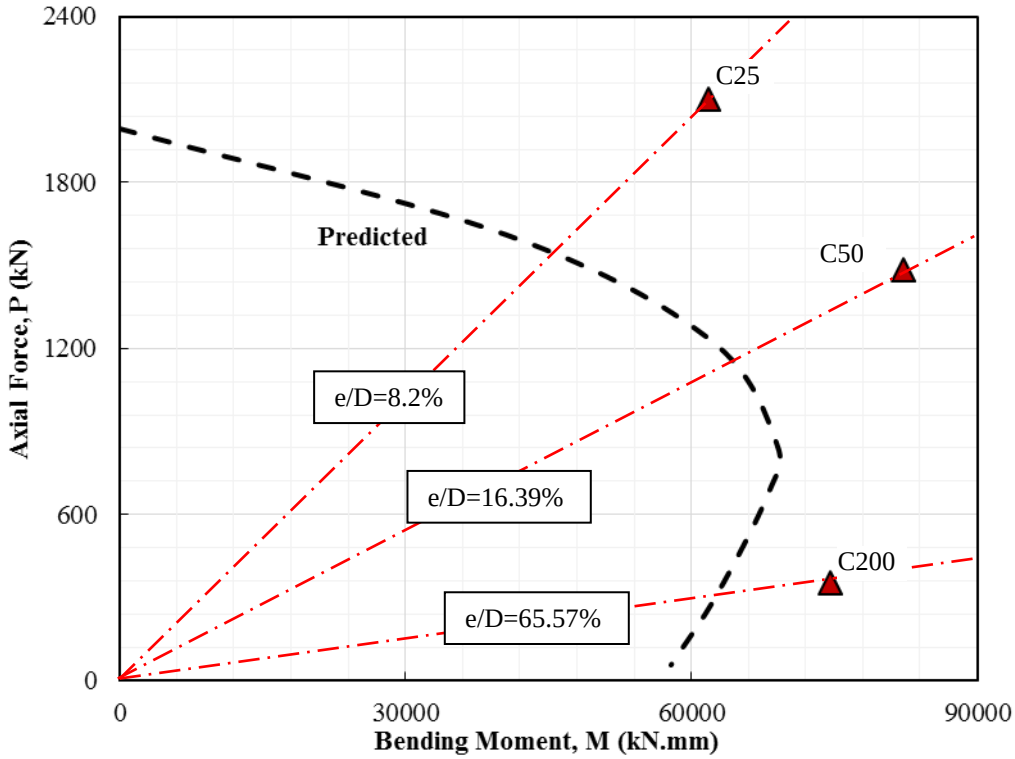

Figure 5: P-M Interaction Diagram for the GFRP-RC specimens

4. CONCLUSIONS

The experimental results concerning the eccentric behavior of full-scale concrete columns reinforced with GFRP bars and spirals were presented and discussed. The main variable was the eccentricity-to-diameter ratio. A total of 3 full-size circular FRP RC columns of 305mm (12") and 1500 mm (60") were constructed and tested under eccentric compression loading. Based on this study, the main findings can be summarized as follows:

1. The failure mechanism was changeable according to the level of eccentricity applied. The failure mechanism of column specimens tested under small eccentric loading was defined as compression-controlled due to concrete crushing. Meanwhile, the failure of the column specimen tested under high eccentric loading was initiated by mild cover spalling, followed by concrete degradation. The failure of the column, however, cannot simply be characterized by a compression failure, it was rather controlled by the properties of the GFRP bars.

2. The axial stiffness of the eccentric columns decreased with each increase in the eccentricity. The response of the load-axial displacement after the peak showed a distinct deformable manner due to the high ultimate strain of the GFRP bars and spiral. The eccentricity had a significant effect on the ultimate load, as should expect.

3. The developed interaction diagram was similar in shape to the interaction diagrams of the steel-RC columns. The estimation of the axial force and the corresponding bending moment using the stress block provided by the Canadian building codes (CSA CAN S806-12 and CSA CAN A23.3-14), satisfying the forces equilibrium, setting the material resistance factors to the unity and neglecting the contribution of the GFRP bars was conservative. The average ratio of the experimental axial load to the predicted axial load (P_{exp}/P_{pred}) was 1.25.

ACKNOWLEDGMENTS

The authors would like to express their special thanks and gratitude to the Natural Science and Engineering Research Council of Canada (NSERC), the NSERC/Industry Research Chair in Innovative FRP Reinforcement for Concrete Structures, and the Ministère de l'Économie, de la Science et de l'Innovation of Quebec for their financial support, Pultrall Inc. (Thetford Mines, QC), and for the technical help provided by the staff of the structural lab of the Department of Civil Engineering at the University of Sherbrooke.

REFERENCES

Afifi, M., Mohamed, H., and Benmokrane, B. (2013a). Axial Capacity of Circular Concrete Columns Reinforced with GFRP Bars and Spirals. *J. Compos. Constr.*, 18(1): 1943-5614.

Benmokrane, B., El-Salakawy, E., El-Ragaby, A., and Lackey, T. (2006). "Designing and testing of concrete bridge decks reinforced with glass FRP bars." *J. Bridge Eng*., 10.1061/ (ASCE)1084-0702(2006)11: 2(217): 217–229.

Benmokrane, B., El-Salakawy, E., El-Ragaby, A., and El-Gamal, S. (2007). "Performance evaluation of innovative concrete bridge deck slabs reinforced with fiber- reinforced polymer bars." *Can. J. Civ. Eng*., 34(3): 298–310.

Canadian Standards Association (CSA). (2012). Design and construction of building components with fiber reinforced polymers, CAN/CSA S806-14, Rexdale, ON, Canada.

El-Salakawy, E., Benmokrane, B., and Desgagné, G. (2003). "FRP composite bars for the concrete deck slab of Wotton Bridge." *Can. J. Civ. Eng*., 30(5): 861–870.

Hassan, M.; Ahmed, E. A.; and Benmokrane, B., 2013, Punching-Shear Strength of Normal- and High-Strength Concrete Flat Slabs Reinforced with GFRP bars. *Journal of composites for construction*, 17(6): 1943-5614.

Mohamed, H., and Benmokrane, B. (2014). Torsional Moment Capacity and Failure Mode Mechanisms of Concrete Beams Reinforced with Carbon FRP Bars and Stirrups. *J. Compos. Constr.*, 19(2): 1943-5592.

Mohamed, H., and Benmokrane, B. (2016). Reinforced Concrete Beams with and without FRP Web Reinforcement under Pure Torsion. *J. Bridge Eng*., 10.1061:1943-5592.

Pultrall Inc. (2014). www.pultrall.com

Rizkalla, S., Hassan, T., and Hassan, N. (2003). "Design recommendations for the use of FRP for reinforcement and strengthening of concrete structures." Progr. *Struct. Eng. Mater*., 5(1): 16–28.

Tikka, T., Francis, M. and Teng, B. (2010). Strength of Concrete Beam-Columns Reinforced with GFRP Bars. *2nd International Structures Specialty Conference*, Winnipeg, Manitoba

Tobbi, H., Farghaly, A. S., and Benmokrane, B. (2012) "Concrete columns reinforced longitudinally and transversally with glass fiber-reinforced polymers bars." *ACI Struct. J*., 109(4): 1–8.

Xue, W., Hu, X. and FANG, Z. (2014). "Experimental studies of GFRP reinforced concrete columns under static eccentric loading." *CICE 2014*, Vancouver, Canada.

Zadeh, H., and Nanni, A. (2013). "Design of RC columns using glass FRP reinforcement." *J. Compos. Constr*., 10.1061/ (ASCE) CC.1943- 5614.0000354: 294–304.